$watermark-text

$watermark-text

$watermark-text

NIH Public Access
Author Manuscript
J Phys Chem Lett. Author manuscript; available in PMC 2013 November 15.

Published in final edited form as:
J Phys Chem Lett. 2012 November 15; 3(22): 3379–3384. doi:10.1021/jz301650q.

Conformational Sampling of Maltose-transporter Components in Cartesian Collective Variables is Governed by the Low-frequency Normal Modes

H. Vashisth and **C. L. Brooks III***
Department of Chemistry and Biophysics Program, University of Michigan, Ann Arbor, MI

Abstract

We have studied large-scale conformational transitions in the maltose-binding protein, and the nucleotide binding domains of a maltose-transporter using enhanced conformational sampling in Cartesian collective variables (CVs) with temperature-accelerated molecular dynamics (TAMD), and C_α-based elastic network normal mode analysis. Significantly, every functional displacement in the TAMD-generated pathways of each protein could be rationalized via a single low-frequency soft mode, while a combination of 2 to 3 low-frequency modes were found to describe the entire conformational change suggesting that collective functional movement in TAMD trajectories is facilitated by the intrinsically accessible low-frequency normal modes. By applying a harmonic potential to facilitate functional motion in TAMD simulations, we also provide a recipe to reproducibly generate structural transitions in both proteins, which can be used to characterize large-scale conformational changes in other biomolecules.

Keywords

conformational transition; normal mode analysis; elastic network models; temperature-accelerated molecules dynamics; maltose-transporter; enhanced sampling

Large-scale conformational changes in proteins, often ligand-triggered, are associated with many cellular processes such as transport, signal transduction, and catalysis.[1] High-resolution crystallographic data have indeed provided a structural basis for the stable open and closed conformations of various proteins, but the mechanistic details of the observed structural transitions are marginally understood, and have been characterized only in a few cases such as adenylate kinase.[2] Detailed experimental characterization of these functional transitions is challenging because intermediate conformations of a protein along the "activation-pathway" are only transiently populated. In such cases, molecular dynamics (MD) simulations can provide atomistically-resolved details of the conformational ensembles of various proteins in principle, but observing large-scale conformational transitions on reasonable time-scales via unbiased simulations remains difficult due to the underlying free-energy barriers. However, many promising simulation approaches that exploit dimensionality-reduction as a tool to explore the free-energy landscape of proteins in large yet finite collective variables (CVs) have been proposed.[3–5] Temperature-accelerated molecular dynamics (TAMD) is one such target-unbiased technique,[6,7] which was demonstrated by Abrams and Vanden-Eijnden to be useful for large-scale conformational

*To whom correspondence should be addressed brookscl@umich.edu, Phone: (734)-647-6682. Fax: (734)-647-1604.

Supporting Information Available
Simulation set-up and execution details along with results from additional trajectories appear in the supplemental material. This material is available free of charge via the Internet at http://pubs.acs.org/.

$watermark-text

$watermark-text

$watermark-text

sampling of proteins.[8] Specifically, they showed that using a fairly general coarse-graining scheme to partition a protein into subdomains (spatially contiguous groups of residues) and exploring the dynamics of these relatively rigid subdomains by accelerating via high fictitious temperature the Cartesian coordinates of the centers-of-mass (COM) of subdomains as CVs, one can generate an MD trajectory at the physical temperature to achieve enhanced conformational sampling of proteins. However, due to stochastic effects inherent in MD simulations and the diffusive-nature of Cartesian CVs in the scheme proposed by Abrams and Vanden-Eijnden, TAMD trajectories can spend significant simulation time exploring the phase-space locally, and hence not every TAMD simulation may lead to a successful transition.[9] Moreover, it is unclear as to what variables contribute to the success of a TAMD trajectory, and whether these variables are generally accessible to a variety of proteins known to undergo structural reorganization.

Collective motions of proteins have been traditionally analyzed successfully using normal mode analysis (NMA) of equilibrium structures (often in Cartesian space but not limited to) because normal modes solely arising from the structure are intrinsically accessible to proteins and collective protein dynamics can usually be described by the low-frequency end of the mode spectrum.[10–15] Particularly, normal mode analyses of coarse-grained (usually C_α-based) elastic network models (ENMs) of proteins[16] with a single-parameter potential[17] and its variants have been remarkably successful in describing large-scale conformational transitions in many biological complexes.[18–29] Given the well-tested ability of normal modes to describe collective motions, we hypothesized that such low-frequency normal modes may significantly contribute to successful collective functional movement during TAMD trajectories, especially when conformational sampling is carried out at least in Cartesian CVs. In this work, we aim to test this proposition by studying open to closed conformational changes in two different proteins that are components of an ATP-binding cassette (ABC) maltose-transporter: (a) maltose-binding protein (MBP), and (b) intracellular nucleotide-binding domains (NBD) (top panels in Figure 1 *a* and *b*). We first conducted four independent all-atom explicit-solvent TAMD simulations with different initial conditions for each protein (Figure S1), and then analyzed these trajectories using C_α-based elastic network NMA of each protein (methodological details appear in the supplemental material).

In Figure 1 (bottom panels), we show individual and cumulative projections or overlaps (θ_m) for 20 low-frequency (non-zero) normal modes of the open conformation of each protein onto the functional displacement vector ($\vec{d}$) computed between the initial and final crystal structures (projection of the nth mode θ_{m_n} is the normalized scalar product between the eigen vector ($\vec{d}_n$) of the corresponding mode and functional displacement $\vec{d}$ i.e. $\theta_{m_n} = \vec{d}_n \cdot \vec{d}/(|\vec{d}_n| \times |\vec{d}|)$; cumulative overlap is then $\sqrt{\theta_{m_1}^2+\theta_{m_2}^2+\cdots+\theta_{m_n}^2}$). In the case of MBP, we observe that the first two low-frequency normal modes have overlaps of $\theta_{m_1} \approx 0.67$ and $\theta_{m_2} \approx 0.68$ respectively, giving a cumulative overlap of ≈0.96, while all 20 low-frequency modes have cumulative overlap of ≈0.97. For NBD, we observe that the overlap of the lowest-frequency mode is $\theta_{m_1} \approx 0.73$, while cumulative overlaps for the first four and all 20 modes are ≈0.96 and ≈0.98, respectively. These data collectively suggest that a few low-frequency normal modes (2 for MBP and 4 for NBD) can account for the entire functional displacement in each protein, which is consistent with what has been observed previously for many proteins.[13] However, it is not yet clear whether the same low-frequency modes contribute to the pathway generated via an all-atom explicit-solvent TAMD simulation, which we discuss in the following.

As pointed out above, TAMD trajectories spend most of their simulation time exploring the phase-space locally, while collective functional excursions can occur nearly stochastically at any time-point during the simulation. This behavior is evident in independent TAMD

$watermark-text

$watermark-text

$watermark-text

trajectories of the open-state of MBP as shown by the root-mean squared deviation (RMSD; C_α) from the known closed crystal structure measured as a function of simulation time (Figure S2; red circles). We therefore prune each TAMD trajectory to extract conformations experiencing functional movement as follows: those frames which have positive functional overlap (θ_f), measured as the scalar product between the displacement vector for each frame of the trajectory with respect to the initial open structure and the functional displacement vector ($\vec{d}$) computed from initial to final crystal structure, are chosen. For MBP, we show values of the functional overlap (θ_f) from these frames plotted against the corresponding RMSD (with respect to the closed crystal structure) in Figure 2*a* (blue; beginning, and red; end of the trajectory). This plot shows that the functional overlap (θ_f) is directly correlated with RMSD, the higher the value of θ_f (suggesting significant functional movement), the lower is the RMSD to known active state and vice versa. Such correlation is consistently observed in independent open-state TAMD trajectories of MBP (Figure S3). Using the C_α-based elastic network NMA (see supplemental methods), we further compute the cumulative overlap of the eigen-vectors of the first two low-frequency normal modes ($\sqrt{\theta_{m_1}^2+\theta_{m_2}^2}$) of the inactive MBP with functionally important displacements, characterized by θ_f, for each TAMD trajectory. We observe a remarkably high cumulative contribution of both modes to functionally important displacements occurring in TAMD trajectories (Figure 2*b* and Figure S3). Furthermore, cumulative overlap of both modes almost linearly grows with high θ_f (Figure 2*b*), suggesting that the higher the functional movement in a TAMD trajectory the more it is characterized by the two low-frequency soft modes of this system. However, not both modes always contribute simultaneously to functionally relevant motion in a TAMD trajectory as shown in Figure 2*c* (red; high θ_f, and blue; low θ_f). Portions of TAMD trajectory where functional movement is significant (gray background marked by circled digits in Figure 2*c*), both modes 1 and 2 contribute to part ①, only mode 1 contributes to part ②, only mode 2 contributes to part ③, and both contribute to part ④ with the contribution of mode 1 relatively higher than mode 2. It is possible for both modes to contribute simultaneously or individually because structural deformation along each of the modes 1 and 2 represents the functionally observed (from crystal structures) closing motion of each lobe of MBP (Figure S1*c*). Overlap of remaining 18 low-frequency normal modes to large-scale functional movement in this TAMD trajectory is insignificant (Figure S4) with similarly consistent observations in independent trajectories (Figure S5–S7).

For the second example, we conducted four independent TAMD trajectories of the open state of NBD (see supplemental methods and Figure S8 for RMSD evolution during each simulation), and pruned these trajectories similar to MBP where frames with positive functional overlap (θ_f) are chosen (*vide surpa*). Such frames represent collective functional displacements in TAMD trajectories. We find that modes 1, 3, and 4 from the low-frequency end of the mode-spectrum (bottom panel in Figure 1*b*) contribute most (though not always simultaneously) to the significant functional motion observed in four TAMD trajectories (gray background marked by circled digits in Figure 3). In run#1 (Figure 3*a*), mode 1 best represents significant functional movement in part ①, while modes 3 and 4 contribute to motion in part ②. In run#2 (Figure 3*b*), both modes 3 and 4 contribute significantly to functional movement in part ①, while the contribution of mode 1 is in-significant in this trajectory. Furtheremore, only mode 1 contributes to part ① in run#3 (Figure 3*c*), while in run#4 (Figure 3*d*), both modes 1 and 3, and not mode 4, contribute to significant functional motion in part ①. Similar to what we saw for MBP, cumulative overlap of modes 1, 3, and 4 ($\sqrt{\theta_{m_1}^2+\theta_{m_3}^2+\theta_{m_4}^2}$) in each TAMD run shows that the higher the functional displacement in a TAMD trajectory the more it is characterized by these three low-frequency modes (Figure S9). The remaining 17 low-frequency modes do not contribute as significantly to large collective functional displacements during the TAMD trajectories (see Figures S10–S13 for

$watermark-text

$watermark-text

$watermark-text

overlaps of all 20 modes in each simulation). Deformation of the open-state structure of NBD along each of the modes 1, 3, and 4 displays the following (Figure S1*f*): mode 1 represents closing motion of two diagonally-placed helical domains of the NBD dimer, mode 3 represents closing motion of the helical domain and the RecA-like domain situated on the same side of the NBD dimer, and mode 4 represents closing motion of two diagonally-placed RecA-like domains of the NBD dimer.

To analyze whether the observed functional contribution of each of the modes 1, 3, and 4 (Figure 3) in the TAMD trajectories is commensurate with the type of collective motion these modes represent (Figure S1*f*), we used a coarse-grained (subdomain centers-of-mass based) mapping of the NBD dimer (Figure 4) to measure inter-subdomain distances (Figure 5).

Specifically, we observe that both helical domains approach each other between 3 to 7 ns in run#1 as indicated by the 2-2′ distance (Figure 5*a*) suggesting that this movement can be characterized by mode 1 alone as seen (Figure 3*a*). Also in the same run, we observe decreasing distances between both RecA-like domains (Figure 5*b*), and between one RecA-like domain and a helical-domain on the same side of the NBD dimer (Figure 5*c*). This suggests the additional contribution of modes 3 and 4 in run#1 as discussed above (Figure 3*a*). In run#2, we briefly observe closing motion between the RecA-like domain and the helical-domain on the same side of NBD dimer (Figure 5*d*) concomitant with higher overlap of mode 3 (Figure 3*b*), and also a sharp closing of both RecA-like domains (Figure 5*e*) consistent with increasing overlap of mode 4 in this functional displacement (Figure 3*b*). The decreasing distance between both helical domains in run#3 (Figure 5*f*) is also characterized by mode 1 as indicated by its higher overlap (Figure 3*c*). Closing of subdomains in run#4 (Figure 5*g* and *h*) is also consistent with observed overlap of respective modes 1 and 3 (Figure 3*d*).

Given that the functional overlap (θ_f) is correlated with the RMSD from the target structures during TAMD simulations, we hypothesized that the likelihood of observation of a large-scale conformational transition in a TAMD trajectory may be significantly increased by adding a biasing-potential to maintain a lower cosine of angle (thereby a higher θ_f) between the instantaneous functional movement and the known functional displacement from crystal structures (see Figure S14 for illustration). To test this, we implemented an angle-dependent harmonic restraining potential on the centers-of-mass of subdomains (see Supplemental Methods) to enhance the conformational search via TAMD simulations. Using this implementation, we carried out multiple independent steered TAMD (sTAMD) simulations of both proteins that remarkably always lead to successful structural transitions unlike TAMD simulations where successful transitions are not guaranteed.[9]

Specifically, we show the C_α-RMSD traces (w. r. t. the closed crystal structure) for two different sTAMD runs of MBP in Figure 6*a*. Starting with the open conformation of MBP, we observe that both sTAMD simulations find the target crystal conformation of MBP within ~3 ns resulting in target RMSD values of ~1 Å. This behavior is consistently observed in 9 additional independent sTAMD simulations of MBP (Figure S15). It is noteworthy because an order-of-magnitude longer TAMD simulations (Figure S2) could not generate this conformational change to the extent observed in the sTAMD simulations. On analyzing these trajectories using elastic network-based NMA, we find that both low-frequency normal modes of MBP (θ_{m1} and θ_{m2}) contribute significantly throughout each sTAMD simulation (red and cyan traces in Figure 6*b and c*), and jointly describe nearly the entire conformational change as indicated by their cumulative overlaps (black traces in Figure 6*b and c*). The contribution of remaining 18 low-frequency normals modes is insignificant in both sTAMD simulations (Figures S16 and S17). The structural changes in

$watermark-text

$watermark-text

$watermark-text

MBP are also highlighted in snapshots at various time-points during sTAMD run#1 in Figure 6*d*.

We further conducted multiple independent sTAMD simulations for NBD starting with its open conformation. For two different sTAMD simulations of NBD, we show the C_α-RMSD traces (w. r. t. the closed crystal structure) in Figure 7*a*. Both simulations successfully generated opened closed structural transitions in NBD within ~4-ns and at target RMSD values of ~2 Å. We observe this structural transition consistently in 14 additonal sTAMD simulations (Figure S18). In comparison to sTAMD simulations, TAMD simulations of NBD perform poorly in capturing this structural transition on time-scales of ~15 ns (see black RMSD traces in Figure S8). As indicated by traces in Figure 7*b and c*, the NMA analyses of these two trajectories show significant individual and cumulative overlaps of two low-frequency normal modes of NBD (θ_{m1} and θ_{m3}) in each sTAMD simulation. However, the contributions of the remaining 18 low-frequency normal modes of NBD in both sTAMD simulations are not as significant (Figures S19 and S20). We also observe that the contributions of modes 1 and 3 are commensurate with the type of structural deformation characterized by each (Figure S1*f*). Consistent with the observed overlap of mode 1 (θ_{m1}), we see decreasing distances between both helical domains of the NBD dimer (see Figure 4), which move by ~10 Å in each sTAMD simulation (left panels in Figure 7*d and e*). Moreover, the concomitant approach of the RecA-like domains and the helical domains located on the same side of the NBD dimer (see Figure 4) is indicated by the decreasing distances between their centers-of-mass (middle and right panels in Figure 7*d and e*), a motion characterized by mode 3. The snapshots of this structural transition from sTAMD run#1 are also highlighted in Figure 7*f* at various time-points.

In summary, we have studied large-scale conformational transitions in the maltose-binding protein, and the nucleotide binding domains of a maltose-transporter using enhanced conformational sampling with temperature-accelerated MD, and C_α-based elastic network normal mode analysis. We conducted multiple explicit-solvent atomistic TAMD simulations of each protein with subdomain centers-of-mass as Cartesian collective variables (CVs), and dissected the diverse collective functional movements in these trajectories by computing the overlap coefficients (normalized scalar product) for 20 low-frequency normal modes. Remarkably, for each protein, every functional displacement in the TAMD-generated pathways could be rationalized via a single low-frequency soft mode, while a combination of 2 to 3 low-frequency modes were found to describe the entire conformational change. This is significant because it directly suggests that large-scale conformational sampling of proteins in Cartesian CVs can be described by the intrinsically accessible low-frequency modes of these proteins. Although our work has only considered Cartesian CVs in TAMD simulations, we point out that the application of TAMD is not limited to only Cartesian CVs, but can be any geometric parameter such as the distance, torsion-angle, or radius of gyration, etc. We further demonstrate that the conformational search via TAMD simulations can be significantly increased by steering/guiding such trajectories using an angle-dependent harmonic potential, which restrains the angle between instantaneous functional movement and the functional displacement known from the crystal structures. We conduct multiple sTAMD simulations of both proteins (MBP and NBD), and find in each case that the structural transition can be reproducibly generated via sTAMD simulations, and also can be characterized by a few low-frequency normal modes. In this context, we also point out that diffusive large-scale motions in proteins have been successfully studied earlier with the help of low-frequency normal modes and MD simulations.[30,31] We note that the characterization of structural transitions in the components of maltose transporter, as done here, is useful to begin constructing functional models of the entire transporter, because it is the coupling of transmembrane motifs with maltose-binding protein (MBP) on the periplasmic side and the nucleotide-binding domains (NBD) on the cytoplasmic side that drives the transport of sugar

(maltose) molecules across the membrane. We suggest that sTAMD simulations may be a useful tool to generate transition pathways between experimentally characterized structural states of other proteins.

Supplementary Material

Refer to Web version on PubMed Central for supplementary material.

Acknowledgments

This work was supported by the NIH resource Multiscale Modeling Tools for Structural Biology (grant RR012255 to CLB) and the NSF funded Center for Theoretical Biological Physics (grant PHY0216576 to CLB).

References

1. Grant BJ, Gorfe AA, McCammon JA. Large Conformational Changes in Proteins: Signaling and Other Functions. Curr Op Struct Biol. 2010; 20:142–147.
2. Arora K, Brooks CL III. Large-scale Allosteric Conformational Transitions of Adenylate Kinase Appear to Involve a Population-shift Mechanism. Proc Natl Acad Sci USA. 2007; 104:18496–18501. [PubMed: 18000050]
3. Laio A, Parrinello M. Escaping Free-energy Minima. Proc Natl Acad Sci USA. 2002; 99:12562–12566. [PubMed: 12271136]
4. Laio A, Gervasio FL. Metadynamics: A Method to Simulate Rare Events and Reconstruct the Free Energy in Biophysics, Chemistry and Material Science. Rep Prog Phys. 2008; 71:126601.
5. Vanden-Eijnden E. Some Recent Techniques for Free Energy Calculations. J Comput Chem. 2009; 30:1737–1747. [PubMed: 19504587]
6. Maragliano L, Vanden-Eijnden E. A Temperature Accelerated Method for Sampling Free Energy and Determining Reaction Pathways in Rare Events Simulations. Chem Phys Lett. 2006; 426:168–175.
7. Maragliano L, Vanden-Eijnden E. Single-sweep Methods for Free Energy Calculations. J Chem Phys. 2008; 128:184110. [PubMed: 18532802]
8. Abrams CF, Vanden-Eijnden E. Large-scale Conformational Sampling of Proteins Using Temperature-accelerated Molecular Dynamics. Proc Natl Acad Sci USA. 2010; 107:4961–4966. [PubMed: 20194785]
9. Vashisth H, Maragliano L, Abrams CF. “DFG-flip” in the Insulin Receptor Kinase is Facilitated by a Helical Intermediate State of the Activation Loop. Biophys J. 2012; 102:1979–1987. [PubMed: 22768955]
10. Hayward S, Go N. Collective Variable Description of Native Protein Dynamics. Ann Rev Phys Chem. 1995; 46:223–250.
11. Berendsen HJC, Hayward S. Collective Protein Dynamics in Relation to Function. Curr Op Struct Biol. 2000; 10:165–169.
12. Bahar I, Lezon TR, Bakan A, Shrivastava IH. Normal Mode Analysis of Biomolecular Structures: Functional Mechanisms of Membrane Proteins. Chem Rev. 2010; 110:1463–1497. [PubMed: 19785456]
13. Tama F, Sanejouand YH. Conformational Change of Proteins Arising from Normal Mode Calculations. Prot Eng. 2001; 14:1–6.
14. Tama F, Brooks CL III. Symmetry Form and Shape: Guiding Principles for Robustness in Macromolecular Machines. Ann Rev Biophys. 2006; 35:115–133.
15. Yang L, Song G, Jernigan RL. How Well Can We Understand Large-scale Protein Motions Using Normal Modes of Elastic Network Models? Biophys J. 2007; 93:920–929. [PubMed: 17483178]
16. Bahar I, Rader AJ. Coarse-grained normal mode analysis in structural biology. Curr Op Struct Biol. 2005; 15:586–592.
17. Tirion MM. Large Amplitude Elastic Motions in Proteins from a Single-parameter, Atomic Analysis. Phys Rev Lett. 1996; 77:1905–1908. [PubMed: 10063201]

$watermark-text
$watermark-text
$watermark-text

$watermark-text

$watermark-text

$watermark-text

18. Brooks B, Karplus M. Normal Modes for Specific Motions of Macromolecules: Application to the Hinge-bending Mode of Lysozyme. Proc Natl Acad Sci USA. 1985; 82:4995–4999. [PubMed: 3860838]
19. Brooks BR, Janezic D, Karplus M. Harmonic-analysis of Large Systems. 1. Methodology. J Comp Chem. 1995; 16:1522–1542.
20. Tama F, Brooks CL III. The Mechanism Pathway of pH Induced Swelling in Cowpea Chlorotic Mottle Virus. J Mol Biol. 2002; 318:733–747. [PubMed: 12054819]
21. Tama F, Wriggers W, Brooks CL III. Exploring Global Distortions of Biological Macromolecules and Assemblies from Low-resolution Structural Information and Elastic Network Theory. J Mol Biol. 2002; 321:297–305. [PubMed: 12144786]
22. Tama F, Valle M, Frank J, Brooks CL III. Dynamic Reorganization of the Functionally Active Ribosome Explored by Normal Mode Analysis and Cryo-electron Microscopy. Proc Natl Acad Sci USA. 2003; 100:9319–9323. [PubMed: 12878726]
23. Tama F, Miyashita O, Brooks CL III. Flexible Multi-scale Fitting of Atomic Structures into Low-resolution Electron Density Maps with Elastic Network Normal Mode Analysis. J Mol Biol. 2004; 337:985–999. [PubMed: 15033365]
24. Tama F, Miyashita O, Brooks CL III. Normal Mode Based Flexible Fitting of High-resolution Structure into Low-resolution Experimental Data from Cryo-EM. J Struct Biol. 2004; 147:315–326. [PubMed: 15450300]
25. Tama F, Brooks CL III. Diversity and Identity of Mechanical Properties of Icosahedral Viral Capsids Studied with Elastic Network Normal Mode Analysis. J Mol Biol. 2005; 345:299–314. [PubMed: 15571723]
26. Ma JP. Usefulness and Limitations of Normal Mode Analysis in Modeling Dynamics of Biomolecular Complexes. Structure. 2005; 13:373–380. [PubMed: 15766538]
27. Yang Z, Majek P, Bahar I. Allosteric Transitions of Supramolecular Systems Explored by Network Models: Application to Chaperonin GroEL. PLoS Comp Biol. 2009; 5:e1000360.
28. Arora, K.; Brooks, CL, III. Molecular Machines in Biology. Frank, J., editor. Cambridge University Press; New York: 2011. p. 59-77.
29. May ER, Feng J, Brooks CL III. Exploring the Symmetry and Mechanism of Virus Capsid Maturation Via an Ensemble of Pathways. Biophys J. 2012; 102:606–612. [PubMed: 22325284]
30. Isin B, Schulten K, Tajkhorshid E, Bahar I. Mechanism of Signal Propagation Upon Retinal Isomerization: Insights from Molecular Dynamics Simulations of Rhodopsin Restrained by Normal Modes. Biophys J. 2008; 95:789–803. [PubMed: 18390613]
31. Peng C, Zhang L, Head-Gordon T. Instantaneous Normal Modes as an Unforced Reaction Coordinate for Protein Conformational Transitions. Biophys J. 2010; 98:2356–2364. [PubMed: 20483345]

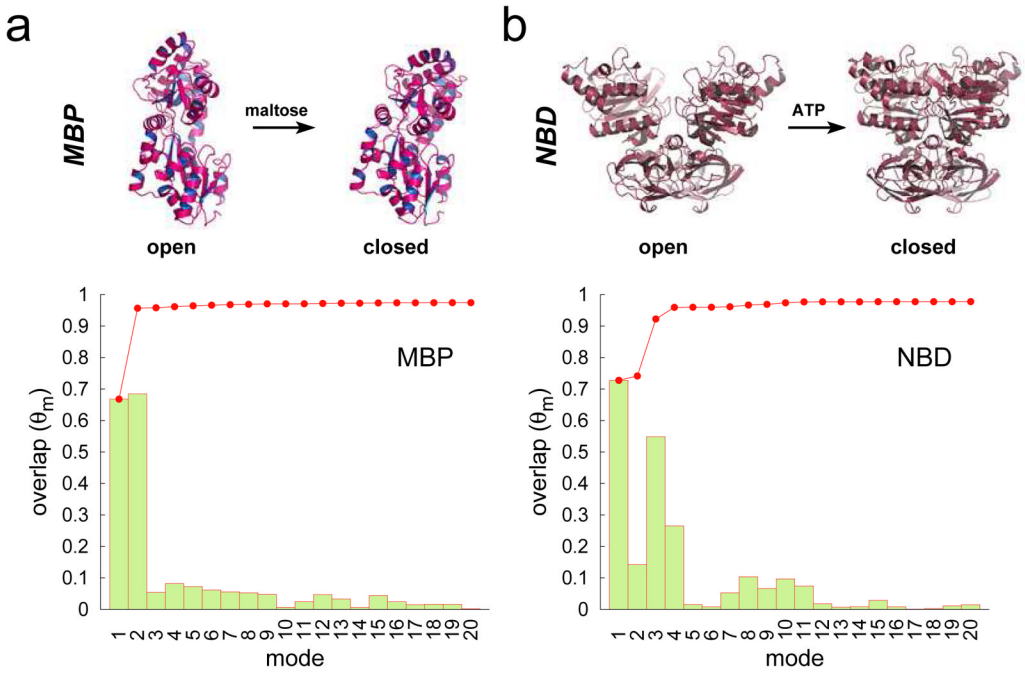

Figure 1.

(*a and b*) Open and closed crystal structures of MBP and NBD (top panels), and individual projections (bars) as well as cumulative projections (red dotted line) of 20 low-frequency normal modes of the open conformation of each protein (bottom panels).

$watermark-text
$watermark-text
$watermark-text

$watermark-text
$watermark-text
$watermark-text

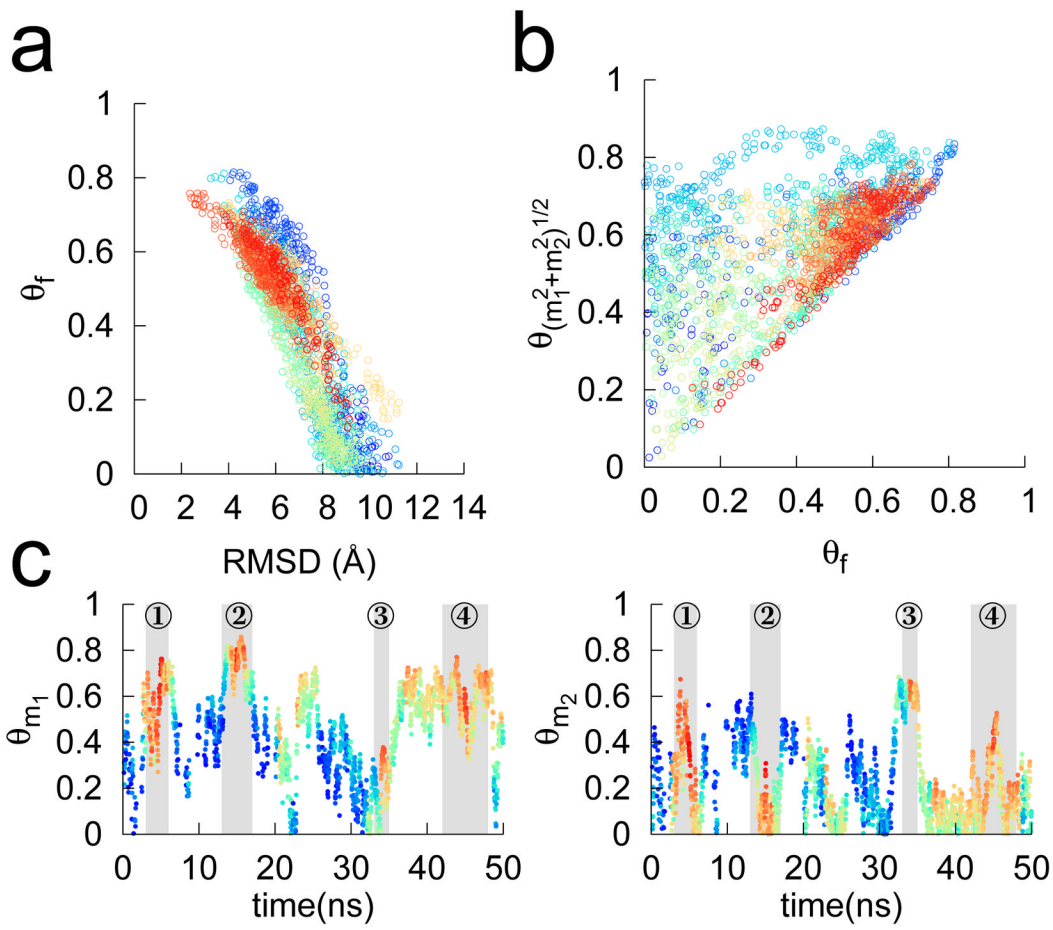

Figure 2.

(*a*) Functional overlap (θ_f) vs. RMSD (relative to the closed state) in a 50-ns TAMD trajectory (run#1) of the open-state of MBP. (*b*) Cumulative overlap of the first two non-zero modes 1 and 2 plotted against θ_f. (*c*) Overlap of each of the modes 1 and 2 with functional displacements during a 50-ns TAMD simulation of MBP. Note that blue indicates the beginning and red the end of TAMD trajectory in panels *a and b*, while red indicates a higher-value of θ_f and blue a lower-value of θ_f in panel *c*.

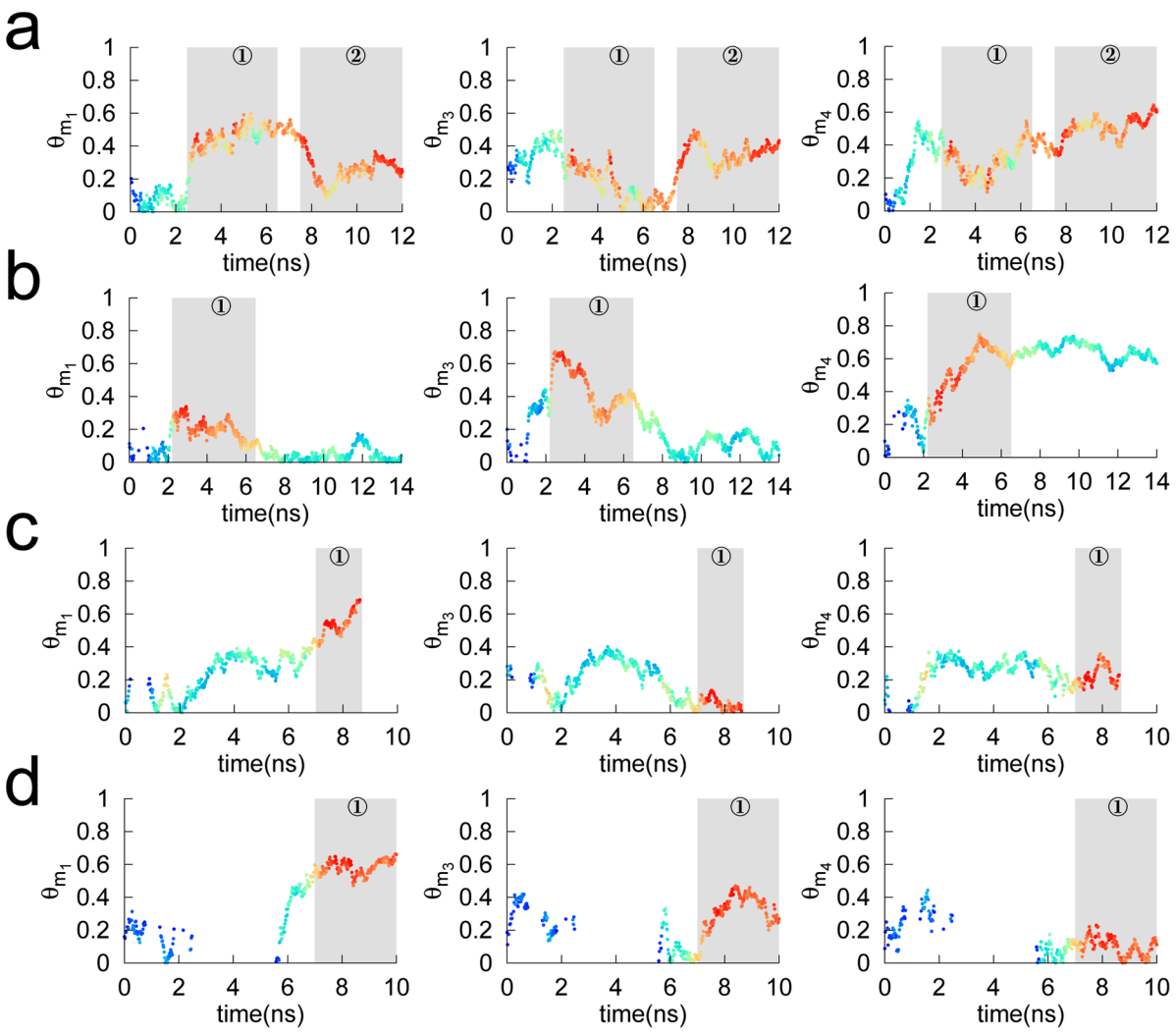

Figure 3.

Overlaps of each of the three non-zero modes 1 (θ_{m1}), 3 (θ_{m3}), and 4 (θ_{m4}) as a function of simulation time (ns) are shown for four different TAMD trajectories of the open-state of NBD. Red indicates a higher-value of functional overlap θ_f and blue a lower-value of θ_f.

$watermark-text
$watermark-text
$watermark-text

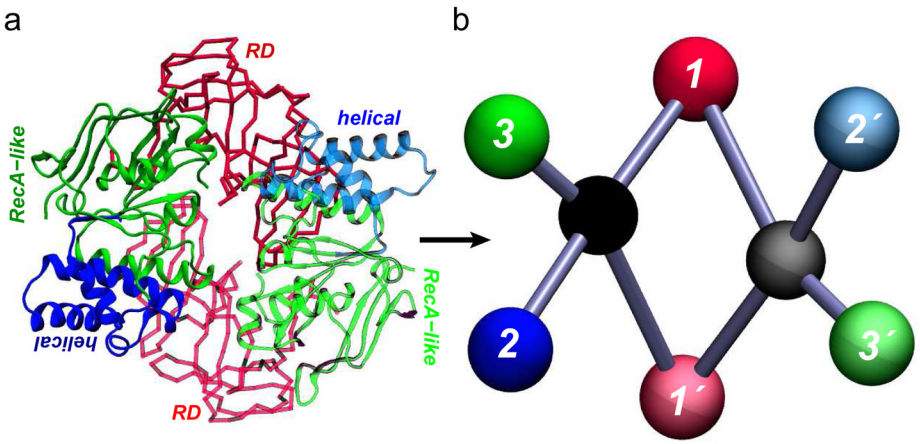

Figure 4.

(*a*) A top-view cartoon representation of the open-state NBD dimer with colored and labeled subdomains. (*b*) Coarse-grained mapping of atomic-structure shown in panel *a*. Each colored bead represents the center-of-mass of corresponding subdomain with hinges as black spheres: 1/1′ the regulatory subdomains (RD), 2/2′ the helical subdomains (helical), and 3/3′ the RecA-like subdomains (RecA-like).

$watermark-text
$watermark-text
$watermark-text

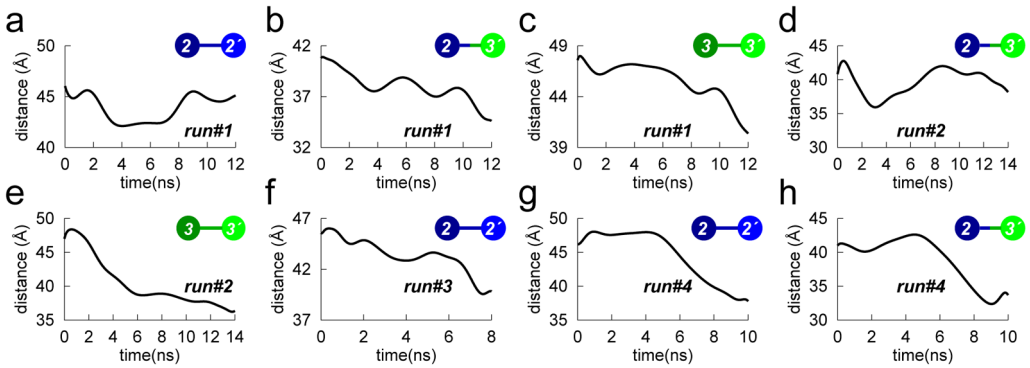

Figure 5.

Selected distances between the centers-of-mass of subdomains represented by coarse-grained beads in Figure 4*b* are shown for four different TAMD trajectories of the open-state of NBD: run#1 (*a, b, and c*), run#2 (*d and e*), run#3 (*f*), and run#4 (*g and h*).

$watermark-text
$watermark-text
$watermark-text

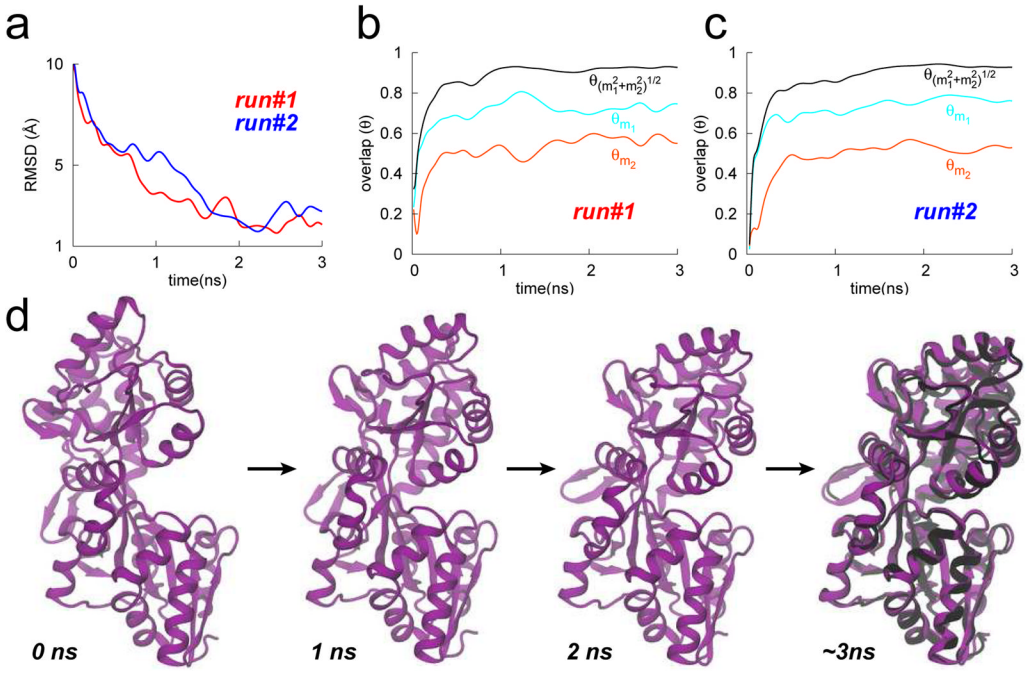

Figure 6.

(*a*) The C_α-RMSD traces (w. r. t. the closed crystal structure) for two different sTAMD runs of MBP. (*b and c*) Cumulative and individual overlaps of modes 1 and 2 as a function of simulation time (ns) are shown for run#1 and run#2 of MBP. (*d*) Representative snapshots of MBP from sTAMD run#1 at different time-points are shown to highlight the structural transition: magenta cartoons (sTAMD-generated conformations) and black cartoon (crystal structure).

$watermark-text
$watermark-text
$watermark-text

$watermark-text
$watermark-text
$watermark-text

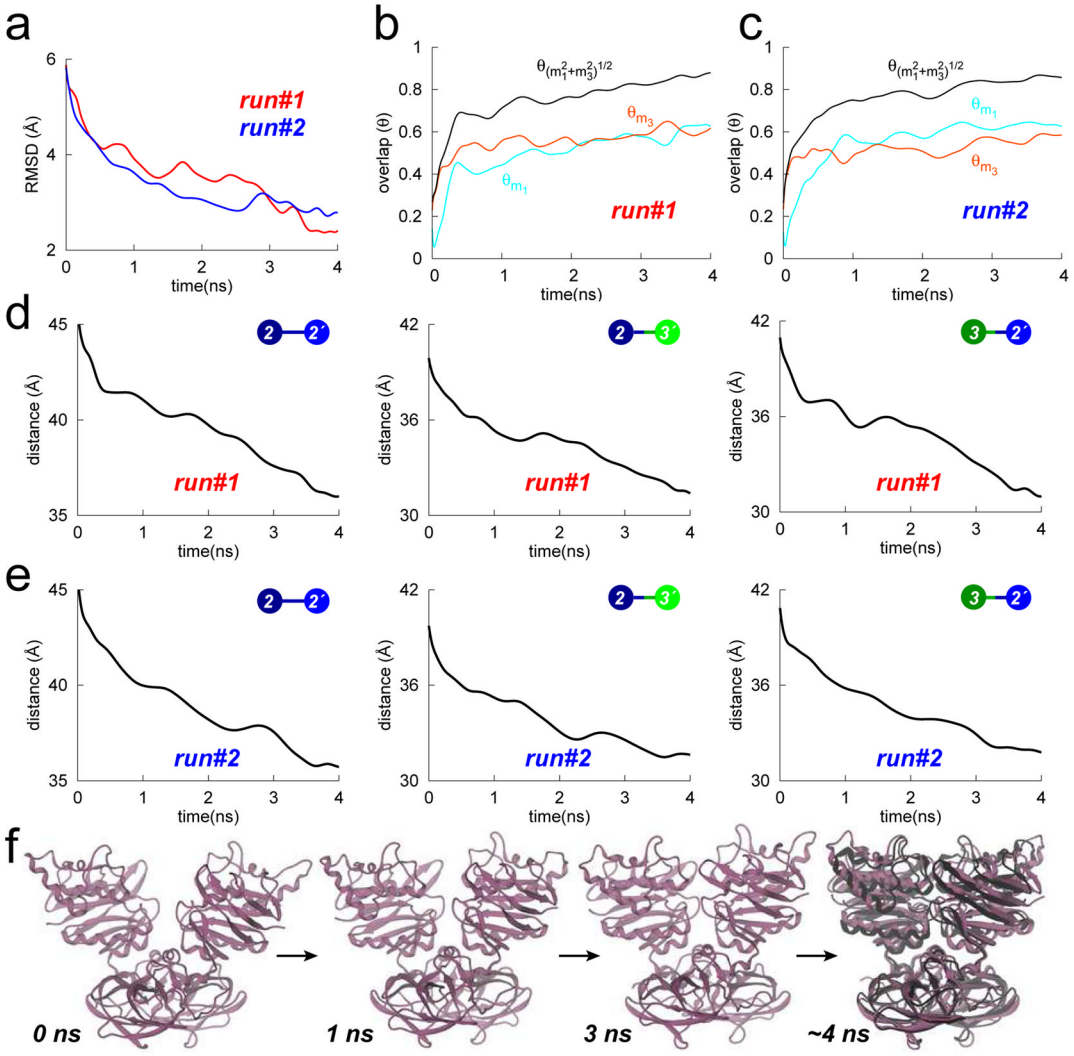

Figure 7.

(*a*) The C_α-RMSD traces (w. r. t. the closed crystal structure) for two different sTAMD runs of NBD. (*b and c*) Cumulative and individual overlaps of modes 1 and 3 as a function of simulation time (ns) are shown for run#1 and run#2 of NBD. (*d and e*) Selected distances between the centers-of-mass of subdomains represented by coarse-grained beads in Figure 4*b* are shown for both sTAMD runs of NBD: run#1 (*d*) and run#2 (*e*). (*f*) Representative snapshots of NBD from sTAMD run#1 at different time-points are shown to highlight the structural transition: magenta cartoons (sTAMD-generated conformations) and black cartoon (crystal structure).